



**Characterizing droughts under current and future climates**

T. Törnros and L. Menzel

This discussion paper is/has been under review for the journal Hydrology and Earth System Sciences (HESS). Please refer to the corresponding final paper in HESS if available.

# Characterizing droughts under current and future climates in the Jordan River region

**T. Törnros and L. Menzel**

Department of Geography, Heidelberg University, Germany

Received: 2 April 2013 – Accepted: 22 April 2013 – Published: 7 May 2013

Correspondence to: T. Törnros (tobias.toernros@geog.uni-heidelberg.de)

Published by Copernicus Publications on behalf of the European Geosciences Union.

[Title Page](#)

[Abstract](#) | [Introduction](#)

[Conclusions](#) | [References](#)

[Tables](#) | [Figures](#)

[⏪](#) | [⏩](#)

[◀](#) | [▶](#)

[Back](#) | [Close](#)

[Full Screen / Esc](#)

[Printer-friendly Version](#)

[Interactive Discussion](#)



## Abstract

The Standardized Precipitation Index (SPI) was applied in order to address the characteristics of current and future agricultural droughts in the Jordan River region located in the southeastern Mediterranean area. In the first step, the SPI was applied on spatially interpolated monthly precipitation data at multiple timescales, i.e. accumulated precipitation was considered over a number of timescales, for example: 1, 3, and 6 months. To investigate the performance of the drought index, correlation analyses were conducted with the Normalized Difference Vegetation Index (NDVI) obtained from remote sensing. The results show that the 6 month SPI best explains the inter-annual variation of the NDVI. Hence, a timescale of 6 months is the most appropriate when addressing agricultural drought in the semi-arid region. In the second step, the 6 month SPI was applied to three climate projections based on the IPCC emission scenario A1B. When comparing the period 2031–2060 with 1961–1990, it is shown that the mean drought duration is projected to increase. Furthermore, the droughts are expected to become more severe because the frequency of severe and extreme droughts is projected to increase and the frequency of moderate drought is projected to decrease. To address the impact of drought on the agricultural sector, the irrigation water demand during drought was simulated with a hydrological model on a spatial resolution of 1 km. A large increase in the demand for irrigation water was simulated, showing that the agricultural sector is expected to become even more vulnerable to drought in the future.

## 1 Introduction

Drought is an extended period with rainfall deficits. In many parts of the world, it is a recurrent natural hazard that has environmental, social and economic impacts (Wilhite, 2005). This wide range of impacts can be simplified and quantified with a drought index. Through such an index, current and past drought events can be compared and essential communication between scientist, decision makers and the public facilitated

# HESSD

10, 5875–5902, 2013

## Characterizing droughts under current and future climates

T. Törnros and L. Menzel

Title Page

Abstract

Introduction

Conclusions

References

Tables

Figures

⏪

⏩

◀

▶

Back

Close

Full Screen / Esc

Printer-friendly Version

Interactive Discussion



## Characterizing droughts under current and future climates

T. Törnros and L. Menzel

Title Page

Abstract

Introduction

Conclusions

References

Tables

Figures

⏪

⏩

◀

▶

Back

Close

Full Screen / Esc

Printer-friendly Version

Interactive Discussion

(Wilhite et al., 2000). Different indices have been used to monitor the spatiotemporal characteristics of soil moisture and drought (Sims et al., 2002; Svoboda et al., 2002; Vergni and Todisco, 2011), and other studies have addressed future drought conditions (Burke and Brown, 2010; Dai et al., 2011; Li et al., 2008). Worldwide, several drought indices are used. The National Oceanic and Atmospheric Administration (NOAA) applies the Palmer Drought Severity Index (Palmer, 1965) and produces monthly maps on the national drought conditions, whereas the Australian Bureau of Meteorology favors the drought index deciles (Gibbs and Maher, 1967). Other well-known drought indices are the Crop Moisture Index (Palmer, 1968) and the Standardized Precipitation Index (SPI), developed by McKee et al. (1993) and applied worldwide, using precipitation data as the only input. Furthermore, it has been recommended by the World Meteorological Organization (WMO, 2011).

The SPI is described in detail by McKee et al. (1993), Guttman (1999) and Bordi et al. (2001). The calculation of the index realizes the fit of a gamma probability distribution function to long-term precipitation data for a given month. Based on the gamma parameters, the cumulative probability of precipitation for the given month can be derived. By applying an approximation, a transformation to a standard normal distribution with the mean value of 0 and standard deviation of 1 can thereafter be conducted. Drought conditions occur when the SPI is negative in an event where the minimum SPI drops below  $-1$  (McKee et al., 1993). In contrast to other drought indices, the SPI can be applied on different timescales (e.g. 1, 3, or 6 months) in order to address different types of droughts, which include meteorological drought (precipitation deficit), hydrological drought (runoff deficit), and agricultural drought (soil moisture deficit), which all are triggered by precipitation deficits with different time lags (McKee et al., 1993).

Several authors have observed a relationship between precipitation and remotely sensed data on vegetation in arid and semi-arid regions (Anyamba and Tucker, 2005; Fabricante et al., 2009; Nezlin et al., 2005; Schmidt and Karnieli, 2000). Positive correlations have also been obtained between drought- and vegetation indices (Ji and Peters, 2003; Quiring and Ganesh, 2010). As such, a correlation shows how vegetation

responds to drought, which supports the performance of the drought index. One of the most used vegetation indices is the Normalized Difference Vegetation Index (NDVI) derived from spectral reflectance in the near-infrared (NIR) and visible red regions according to:

$$5 \quad \text{NDVI} = (\rho_{\text{NIR}} - \rho_{\text{Red}}) / (\rho_{\text{NIR}} + \rho_{\text{Red}}) \quad (1)$$

where  $\rho_{\text{NIR}}$  and  $\rho_{\text{Red}}$  are the reflectance at the NIR and visible red bands. The NDVI can be obtained from the Advanced Very High Resolution Radiometer (AVHRR) and Moderate Resolution Imaging Spectroradiometer (MODIS) sensors among others (Tucker et al., 2005), and be used to estimate biomass and net primary production (Leprieur et al., 2000). Al-Bakri and Taylor (2003) found a correlation between ground-observed biomass data and remotely sensed NDVI in Jordan, and after identifying a positive correlation between precipitation and the NDVI, it has been suggested that a drought index based on precipitation alone is appropriate for the southeastern Mediterranean region (Törnros, 2010). With a well performing drought index, the characteristics of not only current and past drought events can be determined, but in combination with climate projections, future conditions can be addressed.

Several authors have made projections of future changes in the eastern Mediterranean climate by applying Global Climate Models (GCMs) and Regional Climate Models (RCMs). Krichak et al. (2011) applied an ECHAM5/MPI-OM RegCM3 model and noticed a significant trend of decreasing winter precipitation in near coastal areas and an increasing trend in air temperature for all seasons. Samuels et al. (2011) applied the ECHAM5 and HadCM3 GCMs in combination with the RegCM3 and MM5 RCMs. Their results showed that the maximum daily temperature is expected to increase by 2.5–3 °C and that the length of warm and dry spells are expected to be prolonged by 2021–2050 compared with the control period of 1961–1990. Smiatek et al. (2011) applied the ECHAM5-MM5 and HadCM3-MM5 projections and identified a 2.1 °C mean increase of the annual mean temperature by 2031–2060 compared with 1961–1990. They also identified a drop in the annual mean precipitation by 11.5 %. Together, the application

## Characterizing droughts under current and future climates

T. Törnros and L. Menzel

Title Page

Abstract

Introduction

Conclusions

References

Tables

Figures

⏪

⏩

◀

▶

Back

Close

Full Screen / Esc

Printer-friendly Version

Interactive Discussion





**Characterizing droughts under current and future climates**

T. Törnros and L. Menzel

[Title Page](#)[Abstract](#)[Introduction](#)[Conclusions](#)[References](#)[Tables](#)[Figures](#)[⏪](#)[⏩](#)[◀](#)[▶](#)[Back](#)[Close](#)[Full Screen / Esc](#)[Printer-friendly Version](#)[Interactive Discussion](#)

low rainfall recurrently triggers drought events resulting in economic losses, lowered agriculture productivity, reduced stream flow, and falling lake levels (Inbar and Bruins, 2004). In addition, the spatial variability of precipitation is high; convective storms are common and two significant precipitation gradients exist (Ben-Gai et al., 1998). The first gradient is in the west-east direction with higher precipitation in proximity to the Mediterranean Sea (Fig. 1). The hilly regions, stretching from Lebanon in the north to the Gulf of Aqaba in the south, give rise to an orographic lift of moist westerly winds and results in a dry eastern lee side (Dahamsheh and Aksoy, 2007). The second gradient is in the north-south direction. The Golan Heights, stretching northwards from the eastern side of Lake Kinneret, have humid conditions with an annual precipitation of up to 900 mm. Around the Gulf of Aqaba, the conditions are hyper-arid. The area receives dry winds from the Sinai desert and the annual precipitation is less than 50 mm (Dahamsheh and Aksoy, 2007).

In order to characterize droughts in this highly heterogeneous climate region, the study area was divided into three sub-regions. These were defined according to the annual precipitation and refer to arid ( $< 250 \text{ mm yr}^{-1}$ ), semi-arid ( $250\text{--}450 \text{ mm yr}^{-1}$ ) and sub-humid ( $> 450 \text{ mm yr}^{-1}$ ) conditions (Fig. 1). The conditions are unsuitable for rainfed agriculture in the arid sub-region (Bruins, 1999). In the moister sub-regions, rainfed farming is possible only during the winters. This study employed a land use map with a spatial resolution of 1 km, which originated from the Global Land Cover Characterization (GLCC) (Loveland et al., 2000; Menzel et al., 2009). The map is based on the year 2000 and it was assumed that land use had not changed, and will not change in the future. Dominating land uses are shrubland (covering 41 % of the study area), barren land (32 %), mosaic (10 %), which is a mixture between natural vegetation and crops, cropland (9 %), cereals (3 %), grazing land (1 %), grassland (1 %), and urban areas (1 %). As this study focuses on agricultural drought, the study is limited to the three major agricultural classes: cereals, cropland, and mosaic.

## 2.2 Time series of SPI and NDVI

Precipitation was interpolated to a spatial resolution of 1 km by using data obtained for the period 1961–2001 from more than 130 meteorological stations. To account for the strong climatic gradients and an irregular spatial distribution of the stations, a multiple regression analysis, described in detail in Menzel et al. (2009) and Wimmer et al. (2009), was applied. Based on the daily data availability, data characteristics and possible spatial trends, the method automatically identifies a suitable interpolation method (Universal Kriging, Ordinary Kriging, Ordinary Least Squares interpolation or Inverse Distance Weighting) for each day. Thereafter, the interpolated daily precipitation grids were aggregated into monthly totals, which served as input to the SPI.

For the purpose of this study, the SPI source code was provided by the GreenLeaf Project (2012). Their SPI tool was modified to not only work with point data, but also with gridded data where each pixel acts as a single measurement point. In order to identify the most appropriate SPI timescale, the drought index was applied on short timescales (1, 2, and 3 months), moderate timescales (6, 9, and 12 months), as well as long timescales (18 and 24 months). During the SPI calculations, precipitation was then accumulated to this time scale and put into relation with the corresponding period in the long-term precipitation series. As an example, to derive the 3 month SPI value of March 2000 for a pixel, the total precipitation of January, February and March 2000 was compared with long-term time series (1961–2001) of January–March precipitation for the same pixel. The final monthly SPI data set had a spatial resolution of 1 km.

Biweekly NDVI data are available from the Global Inventory Modeling and Mapping Studies (GIMMS) NDVI (Pinzon et al., 2005; Tucker et al., 2005) processed from daily AVHRR images. The global data set has a spatial resolution of 8 km and has been corrected for calibration, view geometry, volcanic aerosols, and other factors not associated with vegetation change. To be compatible with the temporal resolution of the SPI, monthly NDVI were retrieved from the biweekly GIMMS NDVI by computing the average of the two images. In order to address the relationship between the SPI and

**HESSD**

10, 5875–5902, 2013

### Characterizing droughts under current and future climates

T. Törnros and L. Menzel

[Title Page](#)

[Abstract](#)

[Introduction](#)

[Conclusions](#)

[References](#)

[Tables](#)

[Figures](#)

[⏪](#)

[⏩](#)

[◀](#)

[▶](#)

[Back](#)

[Close](#)

[Full Screen / Esc](#)

[Printer-friendly Version](#)

[Interactive Discussion](#)



## Characterizing droughts under current and future climates

T. Törnros and L. Menzel

Title Page

Abstract

Introduction

Conclusions

References

Tables

Figures

⏪

⏩

◀

▶

Back

Close

Full Screen / Esc

Printer-friendly Version

Interactive Discussion

NDVI, a technique applied by Ji and Peters (2003) was applied; the average monthly SPI and NDVI value of all pixels in each land use was determined. Thereafter, the relationship between the two parameters was evaluated according to the correlation coefficient and the  $p$  value. The regression analyses were conducted for the years 1982–2001, because for this period, both precipitation and NDVI data were available. As the summers are completely dry and vegetation shows clear phenological phases, the study was limited to the main growing season (January to May).

### 2.3 Climate projections

Once the most suitable SPI timescale had been identified based on the regression analysis between the SPI and NDVI, data from three climate projections were used as input to the SPI. The Intergovernmental Panel on Climate Change (IPCC) has prepared several emission scenarios in order to address uncertainties in global development. In the present study, we apply the emission scenario A1B, which describes a world with a very rapid economic growth and where energy is generated both from fossil fuels and from alternative energy sources (IPCC, 2007). Three combinations of a GCM and RCM, prepared within the GLOWA Jordan River Project were considered: ECHAM5-MM5 and HadCM3-MM5 (Samuels et al., 2011; Smiatek et al., 2011) delivered from the Institute for Meteorology and Climate Research – Atmospheric Environmental Research (IMK-IFU) in Karlsruhe, Germany and ECHAM5-RegCM3 (Krichak et al., 2010, 2011) delivered from the Tel Aviv University (TAU), Israel. Not all RCMs are appropriate for each region (Krichak et al., 2010). The applied RCMs, however, have been adapted and optimized for the eastern Mediterranean region (Krichak et al., 2005, 2007).

The climate projections have spatial resolutions of 18–25 km. From the projections, daily precipitation data were disaggregated to a spatial resolution of 1 km by applying a linear interpolation between the centre points of each grid cell. Following this, monthly totals were retrieved and the SPI was applied for the years 1961–2060 and evaluated according to current (1961–1990) and future (2031–2060) climates.

## 2.4 Hydrological model

TRAIN is a physically based hydrological model that has focus on the soil-vegetation-atmosphere interface. It is based on comprehensive field studies regarding the water and energy balance of different surface types, including natural vegetation and agricultural land (Menzel, 1997a,b). The model requires input data on precipitation, temperature, wind speed, radiation, and air humidity. These data were available both from meteorological stations and from climate projections, and were prepared just as the precipitation grids. TRAIN also requires information regarding land use and the water holding capacities of the soils. These data were available from the IGBP GLCC (Loveland et al., 2000; Menzel et al., 2009) and Schacht et al. (2011), respectively.

Based on the necessary input data, TRAIN simulates soil moisture, evapotranspiration, snow accumulation/melt, runoff and percolation. For agricultural areas, TRAIN can also deliver information regarding the Irrigation Water Demand (IWD). The model presumes that optimal crop growth takes place when the soil is saturated to field capacity. When the simulated soil moisture drops below a certain threshold level, the model simulates irrigation until optimal plant conditions (field capacity) are reached. The derived IWD is of potential value. In reality, and especially during droughts and water shortages, a sufficient amount of water might not be allocated to agriculture. In the present study, the longest current and future droughts were identified with the SPI. The simulated IWDs during these droughts were thereafter used as an indicator of the drought vulnerability of the region. The higher the IWD, the more threatened the agricultural sector becomes because more water is required to sustain (optimal) vegetation growth.

# HESSD

10, 5875–5902, 2013

## Characterizing droughts under current and future climates

T. Törnros and L. Menzel

[Title Page](#)

[Abstract](#)

[Introduction](#)

[Conclusions](#)

[References](#)

[Tables](#)

[Figures](#)

[⏪](#)

[⏩](#)

[◀](#)

[▶](#)

[Back](#)

[Close](#)

[Full Screen / Esc](#)

[Printer-friendly Version](#)

[Interactive Discussion](#)



### 3 Results

#### 3.1 Spatiotemporal variability of NDVI

To demonstrate the spatial variation of NDVI, the NDVI during vegetation peak in April 2000 is shown in Fig. 2a. It can be seen that vegetation has a spatial pattern that is clearly constrained by precipitation. In the semi-arid and sub-humid areas, the values peak above 0.60, whereas in the arid sub-region the values remain under 0.15. The figure also shows the vegetation phenology throughout the year for the considered land uses (Fig. 2b). By examining the years 1982–2001 and comparing the minimum and maximum mean NDVI (given as a monthly minimum and maximum mean value of all pixels in each land use, respectively), it can be seen that vegetation develops more slowly and reaches a lower maximum for years with unfavorable conditions (as during drought). The difference between the minimum and maximum mean NDVI is highest in the middle of the growing season and during vegetation peak in March/April, whereas the interannual variation is lower during senescence and the dry summer. By conducting regression analyses between NDVI and multiple timescales of the SPI, it was tested whether the drought index could explain these interannual variations in vegetation.

#### 3.2 Correlation of SPI and NDVI

For each considered land use (cereals, cropland, and mosaic), linear correlation analyses were conducted between NDVI and multiple timescales of the SPI for the main growing season (January to May). Figure 3 shows scatter plots of the NDVI and the 1-, 3- and 6 month SPI (the other considered SPI timescales are not plotted here). The results demonstrate that no (significant) correlation is obtained between NDVI and the 1 month SPI. The relationship is only positive in March, during this month the  $p$  value is between 0.61–0.88. It is clear that the 3 month SPI shows a higher correlation with NDVI. The correlation is strongest, and at times significant ( $p < 0.05$ ), in January

Title Page

Abstract

Introduction

Conclusions

References

Tables

Figures

⏪

⏩

◀

▶

Back

Close

Full Screen / Esc

Printer-friendly Version

Interactive Discussion

**Characterizing droughts under current and future climates**

T. Törnros and L. Menzel

[Title Page](#)[Abstract](#)[Introduction](#)[Conclusions](#)[References](#)[Tables](#)[Figures](#)[⏪](#)[⏩](#)[◀](#)[▶](#)[Back](#)[Close](#)[Full Screen / Esc](#)[Printer-friendly Version](#)[Interactive Discussion](#)

and during the vegetation peak in April/May. It can also be seen that a negative relation is obtained in February and March. Furthermore, the results demonstrate that the 6 month SPI is superior to the shorter timescales. Every month induces a positive correlation between the 6 month SPI and NDVI, and at the most, a correlation coefficient of 0.69 is obtained. In January and March, the correlation is significant for cereals, in April it is significant for all land uses, and in May, it is significant for cereals and cropland. For the other months, the relation is strong, but not significant. From all the scatter plots, it can be seen that the relationship between the NDVI and SPI changes with the different states of vegetation growth. In general, it can also be seen that the correlation between the two parameters is strongest around the vegetation peak.

To facilitate the evaluation of all considered SPI timescales, the 15 regression analyses (that were visualized with scatter plots) conducted for each SPI timescale were evaluated with a box plot (Fig. 4). As both the 1 month and the 2 month SPI induce a negative correlation ( $r = -0.21$  and  $r = -0.03$ , respectively) on average, the result once again indicates that the shortest timescales are not capable of addressing agricultural drought. The 3 month SPI has a higher average correlation ( $r = 0.18$ ), which indicates that vegetation responds to precipitation accumulated over several months and that this response is delayed. The same figure shows that all moderate timescales perform almost equally well; the 6-, 9-, and 12 month SPI have an average correlation coefficient of 0.45, 0.44, and 0.42, respectively. However, the value favors slightly the 6 month SPI. The box plot also reveals that the longer timescales have a poorer performance than the moderate timescales; the 18 month SPI has an average correlation coefficient of 0.31 and the 24 month SPI has a corresponding value of 0.28. Altogether, the 6 month SPI best explains the interannual variability of NDVI. Therefore, this timescale was chosen as the most appropriate for assessing agricultural drought in the Jordan River region.

### 3.3 Droughts under current and future climates

To address future droughts, the climate projections for 2031–2060 were used in comparison to 1961–1990. Figure 5 shows the projected changes in annual precipitation. The applied GCM-RCM combinations all simulate a decrease of annual precipitation. For large areas, a decrease of between 10 to 20 % is projected. The ECHAM5-RegCM3 simulates mainly a decrease in the semi-arid and sub-humid regions, whereas both the ECHAM5-MM5 and the HadCM3-MM5 simulate a higher decrease in the southern arid parts. In addition, there are some local areas where increased precipitation is simulated, possible owing to convective rainfall events. Although the spatial distributions of changes in annual precipitation differ slightly between the models, the results can give a sense of the range of the changes expected (Samuels et al., 2011). Furthermore, the projections give indications of a seasonal shift (not shown). Precipitation is projected to increase slightly during October to November, in the beginning of the wet season. During the mid-winter months of December to February, a clear reduction in total precipitation is simulated. For the ECHAM5-RegCM3, the reduction is large for all the mid-winter months, whereas the ECHAM5-MM5 model simulates the strongest reduction in February and none in January. In contrast, the HadCM3-MM5 simulates a reduction in January's precipitation and only minor changes in February. Furthermore, all climate projections predict a decrease in precipitation for March through May.

The SPI results were evaluated according to the duration and frequency of current and future droughts. The drought duration is the number of months with continued drought conditions and the drought frequency is expressed in drought events per decade. For visualization and evaluation purposes, the results from all climate projections were averaged and aggregated according to three sub-regions (Fig. 1), which are referred to as arid, semi-arid, and sub-humid conditions. It is important to notice that because the SPI defines drought according to the deviation from the mean precipitation, the duration of not only future droughts, but also the duration of current droughts might differ between the projections. The results show that the mean duration of current

HESSD

10, 5875–5902, 2013

## Characterizing droughts under current and future climates

T. Törnros and L. Menzel

Title Page

Abstract

Introduction

Conclusions

References

Tables

Figures

⏪

⏩

◀

▶

Back

Close

Full Screen / Esc

Printer-friendly Version

Interactive Discussion

droughts (1961–1990) in the sub-humid, semi-arid, and arid sub-regions is 8 months and 23 days, 8 months and 29 days, and 9 months and 12 days, respectively (Fig. 6a). The mean duration of future droughts (2031–2060) is projected to be 9 months and 27 days, 9 months and 21 days, and 10 months and 28 days in the sub-humid, semi-arid, and arid sub-regions, respectively. Based on a month with 30 days, this is equivalent to an increase of 34 days, 22 days, and 46 days, for the respective sub-regions. In addition, the frequency of current and future droughts were derived and presented as average values revealed from the three climate projections. These were distinguished between moderate (minimum SPI < -1.0), severe (minimum SPI < -1.5), and extreme (minimum SPI < -2.0) drought according to McKee et al. (1993). The number of moderate droughts per decade is expected to decrease in all three sub-regions; from 2.73 to 2.47 in the sub-humid region, from 2.69 to 2.43 in the semi-arid region, and from 2.38 to 2.33 in the arid region (Fig. 6b). Conversely, the number of severe droughts per decade is expected to increase; from 1.44 to 1.80 in the sub-humid region, from 1.43 to 1.81 in the semi-arid region, and from 1.33 to 1.60 in the arid region. Furthermore, the number of extreme droughts per decade is expected to increase; from 0.67 to 1.42 in the sub-humid region, from 0.77 to 1.37 in the semi-arid region, and from 0.71 to 1.30 in the arid region. Altogether, the results show that the average drought is expected to be prolonged and more severe.

### 3.4 Simulated irrigation water demand

The IWD was simulated with TRAIN for the years 1961–1990 and by considering only agricultural land. The latter covers around 22 684 km<sup>2</sup> and comprises vegetables, fruits, cereals, and cropland, as well as a mixture of natural vegetation and crops. The model results show that the annual IWD, in general, does not exceed 100 mm (Fig. 7a). A scattered pattern with values above 200 mm can also be noticed. This pattern is a result of the underlying land use map and the fact that each land use has an individual model parameterization for vegetation (leaf area index, vegetation height, number of vegetation layers, etc.). With more vegetation, transpiration occurs at a higher rate; hence,

# HESSD

10, 5875–5902, 2013

## Characterizing droughts under current and future climates

T. Törnros and L. Menzel

Title Page

Abstract

Introduction

Conclusions

References

Tables

Figures

⏪

⏩

◀

▶

Back

Close

Full Screen / Esc

Printer-friendly Version

Interactive Discussion



more irrigation is simulated in order to supply the crops with water. The average agricultural pixel has an annual IWD of 80 mm, which corresponds to a total water amount of 1815 Mm<sup>3</sup> for all the agricultural land.

5 Additionally, the annual IWD was simulated for drought periods. The results give a value of 122 mm (2770 Mm<sup>3</sup>) and 174 mm (3950 Mm<sup>3</sup>) for the longest current and future drought, respectively (Fig. 7b, c). This implies an increased irrigation demand of 53 % and 118 % compared with average reference conditions. As already mentioned, the IWD is a potential value that in reality and especially during droughts, might not be fulfilled. Therefore, higher values induce higher vulnerability to drought. When examining the spatial distribution of the results, an increase of IWD is seen in the entire study region. The increase is most evident in the semi-arid parts where the annual IWD lies in the range from 100–150 mm during the reference drought, and between 150–200 mm during the future drought period; for specific land uses the values exceed 200 mm. It can also be seen how the northern parts of the study region shows only a small increase of IWD. Altogether, the results demonstrate how the region is expected to become more vulnerable to drought and that the effects will be most evident in regions naturally having drier conditions.

## 4 Discussion

20 The lack of correlation between the 1 month SPI and NDVI is not surprising. After all, a timescale too short, fails to recognize longer periods that are abnormally wet or dry. Furthermore, a time-lag between rainfall and vegetation growth is expected (Ji and Peters, 2003). However, it is interesting to see that the relationship between the 1 month SPI and NDVI tends to be negative. One explanation for this might be that NDVI is more closely related to the rainfall of the previous month, than to the current rainfall. It is also interesting to see that the longer SPI timescales perform worse than the moderate long ones. This indicates that the vegetation growth is not influenced by the previous wet season's rainfall amounts. The reason for this might be linked to the

### Characterizing droughts under current and future climates

T. Törnros and L. Menzel

Title Page

Abstract

Introduction

Conclusions

References

Tables

Figures

⏪

⏩

◀

▶

Back

Close

Full Screen / Esc

Printer-friendly Version

Interactive Discussion



dry summers during which the high cumulative evaporation rate might dry the soils out, irrespective of the soil moisture content at the beginning of the season.

The study also addresses the current and future climates by applying three climate projections. The performance of these climate projections for the current conditions has been evaluated by Samuels et al. (2011). The authors compared the output of the climate models with the same gridded data set on observed precipitation that was applied in the present study. In comparison to observed data, the RCMs tend to underestimate the annual mean precipitation by 5–10 % and slightly overestimate the consecutive dry days. This impacts the simulated IWD among others, particularly when focusing on only one time period e.g. 1961–1990. A major part of the present study, however, is concerned with the change between two time periods. It may be assumable that factors like the underestimation of precipitation affect both time periods equally, and therefore only has a limited influence on our main findings.

The simulated annual IWD of 1815 Mm<sup>3</sup> agrees very well with statistics for the years 2000–2004. For this period, the annual water withdrawal for irrigation and livestock was estimated to be 1129 Mm<sup>3</sup> in Israel, 89 Mm<sup>3</sup> in the Palestinian Authority and 611 Mm<sup>3</sup> in Jordan (FAO, 2009). These numbers add up to a total water withdrawal of 1829 Mm<sup>3</sup>. Nevertheless, there are some uncertainties than can be discussed. Since reliable information regarding irrigation practices are missing, the IWD is simulated based on a pretty simple approach. Furthermore, data regarding multiple cropping and areas equipped for irrigation are in general not available. On the one hand, an overestimation of the area equipped for irrigation would overestimate the IWD and, on the other hand, an underestimation of the areas that are doubled-cropped would underestimate the IWD. These potential erroneous could cancel each other out and still results in a good agreement between the simulated IWD and the statistics. Nonetheless, the model components are up-to-date with our present knowledge of the regional irrigation practices and can be considered plausible.

## HESSD

10, 5875–5902, 2013

### Characterizing droughts under current and future climates

T. Törnros and L. Menzel

Title Page

Abstract

Introduction

Conclusions

References

Tables

Figures

⏪

⏩

◀

▶

Back

Close

Full Screen / Esc

Printer-friendly Version

Interactive Discussion

## 5 Conclusions

In a region where the interannual variability in precipitation is high and drought conditions recurrently occur, the benefits of a well performing drought index are many. A well-known drought index is the SPI. Often, however, the SPI is applied without further considerations to the most appropriate timescale. By conducting correlation analyses between multiple timescales of SPI and NDVI received from remote sensing, it can be seen that the choice of SPI timescale is crucial. A too short timescale fails to recognize longer periods of abnormally wet or dry conditions, and a too long timescale includes redundant information. This study identifies the 6 month SPI as the most appropriate timescale when addressing agricultural drought in the wider Jordan River region. The results are particularly relevant for the project region and the eastern Mediterranean, but also for arid to sub-humid regions in general. The chosen approach could also be employed when evaluating the performance of other drought indices.

For the development of a long-term regional water plan and the preparedness for drought, information regarding future drought conditions is valuable. The hydrological response to a changing climate can be addressed by applying the SPI and a hydrological model on data received from several GCM/RCM combinations. The results of this study give that the future droughts are projected to become more intense because a shift from moderate drought to severe and extreme drought is expected to occur in southeastern Mediterranean region. It is shown that the intensified droughts lead to large increases in the annual IWD. Hence, the agricultural sector is expected to become even more vulnerable to drought in the future. Although this study focuses on agricultural droughts, the results are also valuable regarding; exacerbated land degradation (WMO, 2005), biodiversity (Chase, 2005; Kutiel et al., 2000), livestock raising (Meir and Tsoar, 1996), river flows and lake levels (Inbar and Bruins, 2004), as well as aquifer recharge and the salinization of groundwater (Bruins, 1999), all of which are impacted negatively by drought. This also applies to the arid sub-region where agriculture is only practiced to a limit extent.

## Characterizing droughts under current and future climates

T. Törnros and L. Menzel

[Title Page](#)

[Abstract](#)

[Introduction](#)

[Conclusions](#)

[References](#)

[Tables](#)

[Figures](#)

[⏪](#)

[⏩](#)

[◀](#)

[▶](#)

[Back](#)

[Close](#)

[Full Screen / Esc](#)

[Printer-friendly Version](#)

[Interactive Discussion](#)



*Acknowledgements.* This study was conducted within the GLOWA Jordan River project funded by the German Ministry of Education and Research (BMBF), contract number 01LW05091. The authors are grateful to Stefan Schläffer for providing spatially interpolated climate data.

## References

- 5 Al-Bakri, J. T. and Taylor, J. C.: Application of NOAA AVHRR for monitoring vegetation conditions and biomass in Jordan, *J. Arid Environ.*, 54, 579–593, 2003.
- Anyamba, A. and Tucker, C. J.: Analysis of Sahelian vegetation dynamics using NOAA-AVHRR NDVI data from 1981–2003, *J. Arid Environ.*, 63, 596–614, 2005.
- 10 Ben-Gai, T., Bitan, A., Manes, A., Alpert, P., and Rubin, S.: Spatial and temporal changes in rainfall frequency distribution patterns in Israel, *Theor. Appl. Climatol.*, 61, 177–190, 1998.
- Bordi, I., Frigio, S., Parenti, P., Speranza, A., and Sutera, A.: The analysis of the standardized precipitation index in the Mediterranean area: large-scale patterns, *Ann. Geofis.*, 44, 965–978, 2001.
- Bruins, H. J.: Drought management and water supply systems in Israel, in: *Drought Management Planning in Water Supply Systems*, edited by: Cabrera, E. and García-Serra, J., Kluwer Academic Publishers, Dordrecht, The Netherlands, 299–321, 1999.
- 15 Burke, E. J. and Brown, S. J.: Regional drought over the UK and changes in the future, *J. Hydrol.*, 394, 471–485, 2010.
- Chase, J. M.: Drought mediates the importance of stochastic community assembly, *P. Natl. Acad. Sci. USA*, 104, 17430–17434, 2007.
- Dahamsheh, A. and Aksoy, H.: Structural characteristics of annual precipitation data in Jordan, *Theor. Appl. Climatol.*, 88, 201–212, 2007.
- Dai, A.: Drought under global warming: a review, *Clim. Change*, 2, 45–65, 2011.
- Fabricante, I., Oesterheld, M., and Paruelo, J. M.: Annual and seasonal variation of NDVI explained by current and previous precipitation across northern Patagonia, *J. Arid Environ.*, 73, 745–753, 2009.
- 25 FAO: *Irrigation in the Middle East region in figures – AQUASTAT survey – 2008*, FAO Water Reports 34, Rome, Italy, 423 pp., 2009.
- Gibbs, W. J. and Maher, J. V.: *Rainfall deciles as drought indicators*, Bureau of Meteorology Bulletin, 48, Melbourne, Australia, 1967
- 30

## Characterizing droughts under current and future climates

T. Törnros and L. Menzel

Title Page

Abstract

Introduction

Conclusions

References

Tables

Figures

⏪

⏩

◀

▶

Back

Close

Full Screen / Esc

Printer-friendly Version

Interactive Discussion



## Characterizing droughts under current and future climates

T. Törnros and L. Menzel

Title Page

Abstract

Introduction

Conclusions

References

Tables

Figures

⏪

⏩

◀

▶

Back

Close

Full Screen / Esc

Printer-friendly Version

Interactive Discussion

GreenLeaf Project: The standardized precipitation index, source code, available at: <http://greenleaf.unl.edu/>, last access: 1 March, 2012.

Guttman, N. B.: Accepting the standardized precipitation index: a calculation algorithm, *J. Am. Water Resour. As.*, 35, 311–322, 1999.

Inbar, M. and Bruins, H. J.: Environmental impact of multi-annual drought in the Jordan Kinneret watershed, Israel, *Land Degrad. Dev.*, 15, 243–256, doi:10.1002/ldr.612, 2004.

IPCC (Intergovernmental Panel on Climate Change): Climate change – the physical science basis, in: Contribution of Working Group I to the Fourth Assessment Report of the IPCC, edited by: Solomon, S., Qin, D., Manning, M., Chen, Z., Marquis, M., Averyt, K. B., Tignor, M., and Miller, H. L., Cambridge University Press, Cambridge, UK, 996 pp., 2007.

Ji, L. and Peters, A. J.: Assessing vegetation response to drought in the northern Great Plains using vegetation and drought indices, *Remote Sens. Environ.*, 87, 85–98, 2003.

Krichak, S. O., Alpert, P., and Dayan, M.: Adaptation of the MM5 and RegCM3 for regional, climate modeling over the eastern Mediterranean region, *Geophys. Res. Abstr.*, 7, 04624, 2005.

Krichak, S. O., Alpert, P., Bassat, K., and Kunin, P.: The surface climatology of the eastern Mediterranean region obtained in a three-member ensemble climate change simulation experiment, *Adv. Geosci.*, 12, 67–80, 2007, <http://www.adv-geosci.net/12/67/2007/>.

Krichak, S., Alpert, P., and Kunin, P.: Numerical simulation of seasonal distribution of precipitation over the eastern Mediterranean with a RCM, *Clim. Dynam.*, 34, 47–59, doi:10.1007/s00382-009-0649-x, 2010.

Krichak, S., Breitgand, J., Samuels, R., and Alpert, P.: A double-resolution transient RCM climate change simulation experiment for near-coastal eastern zone of the eastern Mediterranean region, *Theor. Appl. Climatol.*, 103, 167–195, 2011.

Kutiel, P., Kutiel, H., and Lavee, H.: Vegetation response to possible scenarios of rainfall variations along a Mediterranean-extreme arid climatic transect, *J. Arid Environ.*, 44, 277–290, 2000.

Leprieur, C., Kerr, Y. H., Mastorchio, S., and Meunier, J. C.: Monitoring vegetation cover across semi-arid regions: comparison of remote observations from various scales, *Int. J. Remote Sens.*, 21, 281–300, doi:10.1080/014311600210830, 2000.

## Characterizing droughts under current and future climates

T. Törnros and L. Menzel

Title Page

Abstract

Introduction

Conclusions

References

Tables

Figures

⏪

⏩

◀

▶

Back

Close

Full Screen / Esc

Printer-friendly Version

Interactive Discussion

- Li, W., Fu, R. I. R., Juarez, N., and Fernandes, K.: Observed change of the standardized precipitation index, its potential cause and implications to future climate change in the Amazon region, *Philos. T. Roy. Soc. B.*, 363, 1767–1772, 2008.
- Loveland, T. R., Reed, B. C., Brown, J. F., Ohlen, D. O., Zhu, Z., Yang, L., and Merchant, J. W.: Development of a global land cover characteristics database and IGBP discover from 1 km AVHRR data, *Int. J. Remote Sens.*, 21, 1303–1330, 2000.
- McKee, T., Nolan, J., and Kleist, J.: The relationship of drought frequency and duration to time scales, in: *Proceedings of the 8th Conference of Applied Climatology*, 17–22 January, Anaheim, CA, American Meteorological Society, Boston, MA, 179–184, 1993.
- Meir, A. and Tsoar, H.: International borders and range ecology: the case of Bedouin transborder grazing, *Hum. Ecol.*, 24, 39–64, doi:10.1007/bf02167960, 1996.
- Menzel, L.: Modellierung der Evapotranspiration im System Boden-Pflanze-Atmosphäre, *Zür. Geogr. Schr.*, 67, Institute of Geography, ETH Zürich, Zürich, 128 pp., 1997a (in German).
- Menzel, L.: Modelling canopy resistances and transpiration of grassland, *Phys. Chem. Earth*, 21, 123–129, 1997b.
- Menzel, L., Koch, J., Onigkeit, J., and Schaldach, R.: Modelling the effects of land-use and land-cover change on water availability in the Jordan River region, *Adv. Geosci.*, 21, 73–80, 2009, <http://www.adv-geosci.net/21/73/2009/>.
- Nezlin, N. P., Kostianoy, A. G., and Li, B.-L.: Inter-annual variability and interaction of remote-sensed vegetation index and atmospheric precipitation in the Aral Sea region, *J. Arid Environ.*, 62, 677–700, 2005.
- Palmer, W. C.: *Meteorological drought*, Research Paper No. 45, US Department of Commerce Weather Bureau, Washington DC, 1965.
- Palmer, W. C.: Keeping track of crop moisture conditions, nationwide: the new crop moisture index, *Weatherwise*, 21, 156–161, 1968.
- Pinzon, J., Brown, M. E., and Tucker, C. J.: Satellite time series correction of orbital drift artifacts using empirical mode decomposition, in: *Hilbert–Huang Transform: Introduction and Applications*, edited by: Huang, N., World Scientific Publishing, Singapore, 167–186, 2005.
- Quiring, S. and Ganesh, S.: Evaluating the utility of the vegetation condition index (VCI) for monitoring meteorological drought in Texas, *Agr. Forest Meteorol.*, 150, 330–339, 2010.

## Characterizing droughts under current and future climates

T. Törnros and L. Menzel

Title Page

Abstract

Introduction

Conclusions

References

Tables

Figures

⏪

⏩

◀

▶

Back

Close

Full Screen / Esc

Printer-friendly Version

Interactive Discussion

Samuels, R., Smiatek, G., Krichak, S., Kunstmann, H., and Alpert, P.: Extreme value indicators in highly resolved climate change simulations for the Jordan River area, *J. Geophys. Res.*, 116, D24123, doi:10.1029/2011jd016322, 2011.

Schacht, K., Gönster, S., Jüscke, E., Chen, Y., Tarchitzky, J., Al-Bakri, J., Al-Karablieh, E., and Marschner, B.: Evaluation of soil sensitivity towards the irrigation with treated wastewater in the Jordan River region, *Water*, 3, 1092–1111, 2011.

Schmidt, H. and Karnieli, A.: Remote sensing of the seasonal variability of vegetation in a semi-arid environment, *J. Arid Environ.*, 45, 45–59, 2000.

Sims, A. P., Niyogi, D. D. S., and Raman, S.: Adopting drought indices for estimating soil moisture: a North Carolina case study, *Geophys. Res. Lett.*, 29, 24-1–24-4, doi:10.1029/2001GL013343, 2002.

Smiatek, G., Kunstmann, H., and Heckl, A.: High-resolution climate change simulations for the Jordan River area, *J. Geophys. Res.*, 116, D16111, doi:10.1029/2010JD015313, 2011.

Svoboda, M., Lecomte, D., Hayes, M., Heim, R., Gleason, K., Angel, J., Rippey, B., Tinker, R., Palecki, M., Stooksbury, D., Miskus, D., and Stephens, S.: The drought monitor, *B. Am. Meteorol. Soc.*, 83, 1181–1190, 2002.

Törnros, T.: Precipitation trends and suitable drought index in the arid/semi-arid southeastern Mediterranean region, in: *Global Change: Facing Risks and Threats to Water Resources*, Proc. of the Sixth World FRIEND Conference, Fez, Morocco, October 2010, edited by: Servat, E., Demuth, S., Dezetter, A., and Daniell, T., IAHS Publ., 340, 157–163, 25–29 October 2010, Fez, Morocco, 2010.

Tucker, C. J., Pinzon, J. E., Brown, M. E., Slayback, D., Pak, E. W., Mahoney, R., Vermote, E., and El Saleous, N.: An extended AVHRR 8-km NDVI data set compatible with MODIS and SPOT vegetation NDVI data., *Int. J. Remote Sens.*, 26, 4485–5598, 2005.

Vergni, L. and Todisco, F.: Spatio-temporal variability of precipitation, temperature and agricultural drought indices in central Italy, *Agr. Forest Meteorol.*, 151, 301–313, 2011.

Wilhite, D. A. (Ed.): *Drought and Water Crises: Science, Technology and Management Issues*, CRC Press, Boca Raton, FL, 406 pp., 2005.

Wilhite, D., Hayes, M., Knutson, C., and Smith, K. H.: Planning for drought: moving from crisis to risk management, *J. Am. Water Resour. As.*, 36, 697–710, 2000.

Wimmer, F., Schläffer, S., aus der Beek, T., and Menzel, L.: Distributed modelling of climate change impacts on snow sublimation in northern Mongolia, *Adv. Geosci.*, 21, 117–124, 2009, <http://www.adv-geosci.net/21/117/2009/>.

WMO (World Meteorological Organization): Climate and Land Degradation, WMO-No. 989, Geneva, Switzerland, 2005.

WMO: Sixteenth World Meteorological Congress (Cg-XVI), 16 May–3 June 2011, Abridged final report with resolutions, WMO-No. 1077, Geneva, Switzerland, 2011.

## HESSD

10, 5875–5902, 2013

### Characterizing droughts under current and future climates

T. Törnros and L. Menzel

Title Page

Abstract

Introduction

Conclusions

References

Tables

Figures



Back

Close

Full Screen / Esc

Printer-friendly Version

Interactive Discussion

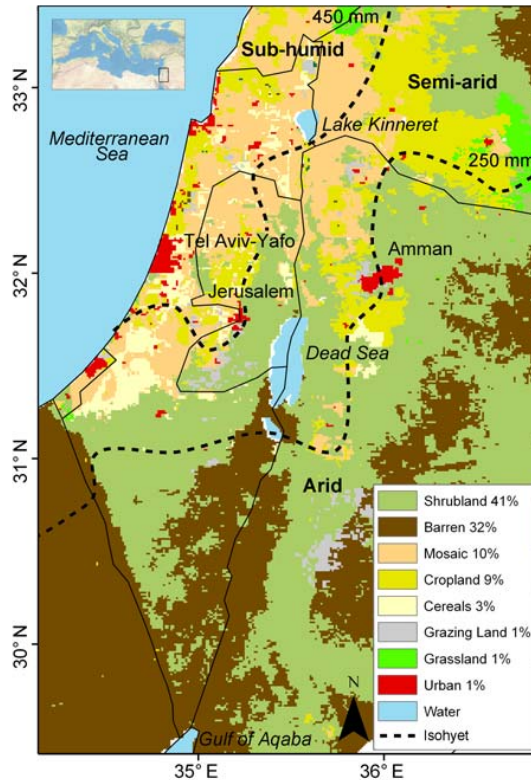


**Fig. 1.** Location of the study region (based on the ESRI World Physical Map) and land uses with spatial coverage in percentages. Also shown are the 250 and 450 mm isohyets derived from spatially interpolated precipitation data. These smoothed lines define a sub-humid, semi-arid and arid sub-region.

## Characterizing droughts under current and future climates

T. Törnros and L. Menzel

[Title Page](#)

[Abstract](#) [Introduction](#)

[Conclusions](#) [References](#)

[Tables](#) [Figures](#)

[⏪](#) [⏩](#)

[⏴](#) [⏵](#)

[Back](#) [Close](#)

[Full Screen / Esc](#)

[Printer-friendly Version](#)

[Interactive Discussion](#)



## Characterizing droughts under current and future climates

T. Törnros and L. Menzel

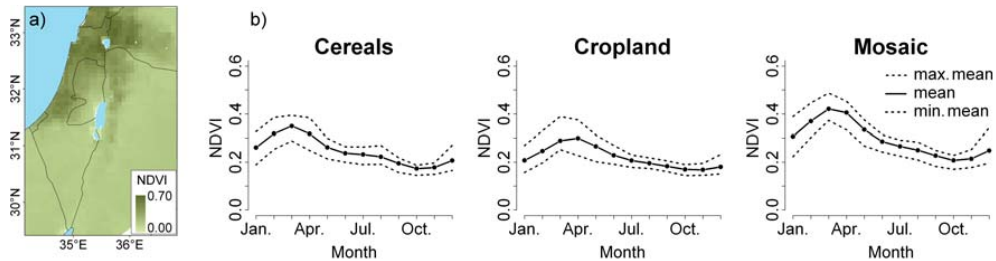


**Fig. 2.** (a) Spatial distribution of NDVI in April 2000, and (b) the NDVI phenology throughout the year for chosen land uses. Shown are the maximum mean NDVI, the mean NDVI, and the minimum mean NDVI based on monthly values for the years 1982–2001.

Title Page

Abstract

Introduction

Conclusions

References

Tables

Figures

⏪

⏩

◀

▶

Back

Close

Full Screen / Esc

Printer-friendly Version

Interactive Discussion

Characterizing droughts under current and future climates

T. Törnros and L. Menzel

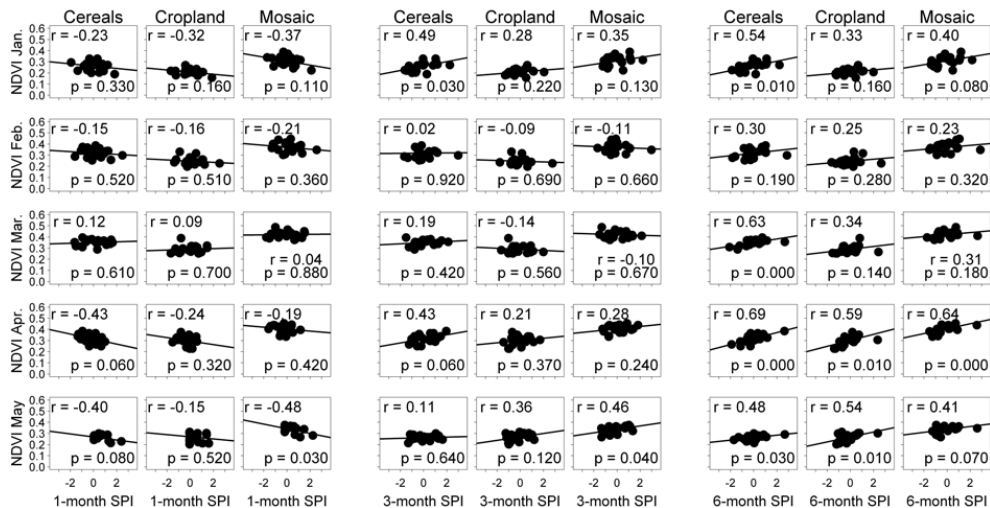


Fig. 3. Scatter plots between NDVI and multiple timescales of SPI for chosen land uses based on the years 1982–2001. Also shown are the correlation coefficient  $r$  and the  $p$  value.

Title Page

Abstract Introduction

Conclusions References

Tables Figures

⏪ ⏩

◀ ▶

Back Close

Full Screen / Esc

Printer-friendly Version

Interactive Discussion



**Characterizing  
droughts under  
current and future  
climates**

T. Törnros and L. Menzel

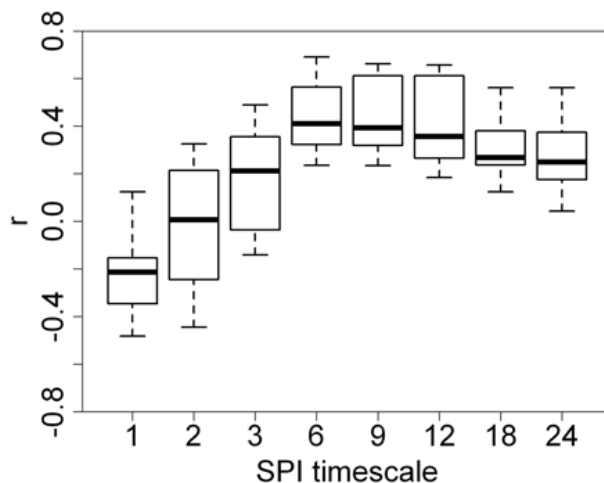


**Fig. 4.** Box plot for the correlation of NDVI and multiple timescales of SPI;  $r$  is the correlation coefficient. The figure is based on the months January to May and the land uses cereals, cropland, and mosaic. Hence, altogether there are 15 values for each SPI timescale.

[Title Page](#)[Abstract](#)[Introduction](#)[Conclusions](#)[References](#)[Tables](#)[Figures](#)[⏪](#)[⏩](#)[◀](#)[▶](#)[Back](#)[Close](#)[Full Screen / Esc](#)[Printer-friendly Version](#)[Interactive Discussion](#)

## Characterizing droughts under current and future climates

T. Törnros and L. Menzel

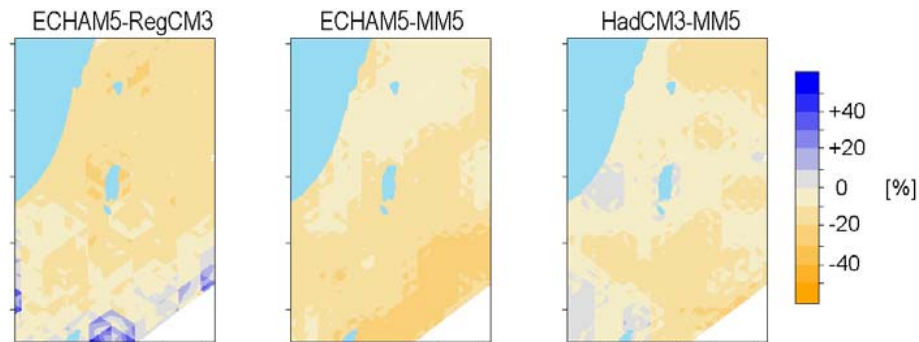


**Fig. 5.** Projected relative changes in annual precipitation simulated by three climate models. The figure shows the period 2031–2060 in comparison with 1961–1990.

[Title Page](#)[Abstract](#)[Introduction](#)[Conclusions](#)[References](#)[Tables](#)[Figures](#)[⏪](#)[⏩](#)[◀](#)[▶](#)[Back](#)[Close](#)[Full Screen / Esc](#)[Printer-friendly Version](#)[Interactive Discussion](#)

## Characterizing droughts under current and future climates

T. Törnros and L. Menzel

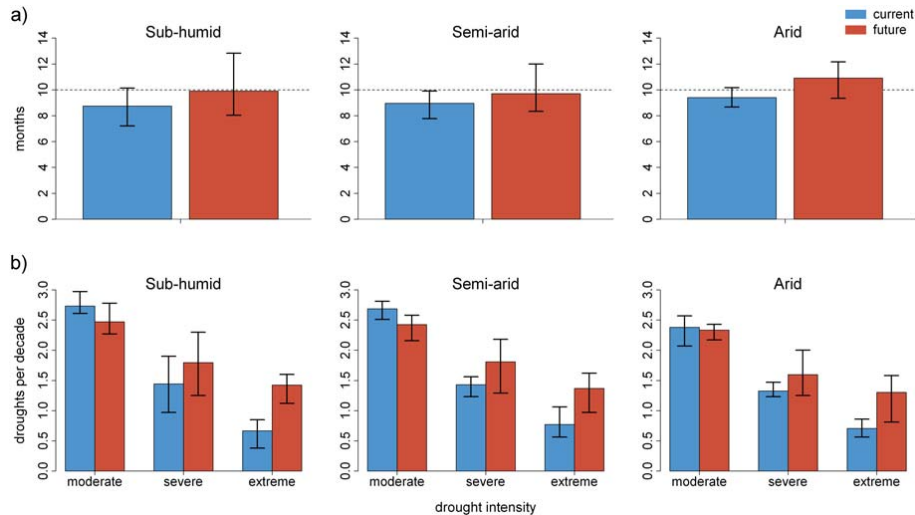


**Fig. 6.** (a) Mean drought duration in months, and (b) drought frequency in droughts per decade for the period 1961–1990 (blue) and 2031–2060 (red). The bars show the mean value from three climate projections, whereas the error-bars show the range between the climate projections.

[Title Page](#)
[Abstract](#)
[Introduction](#)
[Conclusions](#)
[References](#)
[Tables](#)
[Figures](#)
[⏪](#)
[⏩](#)
[◀](#)
[▶](#)
[Back](#)
[Close](#)
[Full Screen / Esc](#)
[Printer-friendly Version](#)
[Interactive Discussion](#)

## Characterizing droughts under current and future climates

T. Törnros and L. Menzel

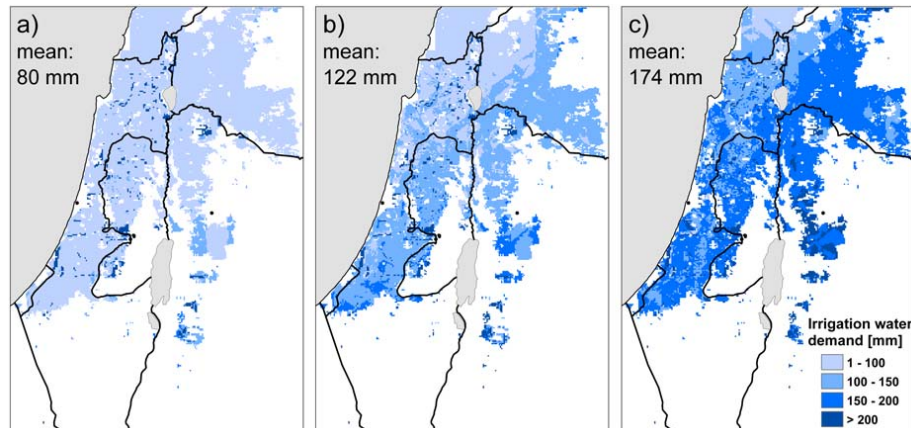


**Fig. 7.** Simulated annual irrigation water demand (IWD) in mm. The figure shows: **(a)** the current reference conditions based on the period 1961–1990, **(b)** the annual IWD during the longest drought in 1961–1990, and **(c)** the annual IWD during the longest drought in 2031–2060. The figure is based on mean values from three climate projections, showing agricultural land only. An assumption of no land use change has been made.

[Title Page](#)[Abstract](#)[Introduction](#)[Conclusions](#)[References](#)[Tables](#)[Figures](#)[⏪](#)[⏩](#)[◀](#)[▶](#)[Back](#)[Close](#)[Full Screen / Esc](#)[Printer-friendly Version](#)[Interactive Discussion](#)